THE JOURNAL OF PHYSICAL CHEMISTRY B

Article

pubs.acs.org/JPCB

Self-Assembly of Amphiphilic Peptide $(AF)_6H_5K_{15}$: Coarse-Grained Molecular Dynamics Simulation

Naresh Thota,[†] Zhonglin Luo,[†,‡] Zhongqiao Hu,[†] and Jianwen Jiang[†,*]

[†]Department of Chemical and Biomolecular Engineering, National University of Singapore, 117576, Singapore

[‡]School of Materials Science and Engineering, Changzhou University, Jiangsu, 213164, People's Republic of China

Supporting Information

ABSTRACT: Amphiphilic peptides are receiving considerable interest for drug delivery because of their self-assembly nature. A molecular dynamics simulation study is reported here to investigate the self-assembly of FA32 peptide composed of 32 amino acid $(AF)_6H_5K_{15}$. The peptide, as well as water and counterions, are represented by the MARTINI coarse-grained model. Within 5 μs simulation duration, the peptide is observed to form micelles. Ala and Phe stay in the hydrophobic core, Lys in the hydrophilic shell, and amphiphilic His at the interface. The assembly process and microscopic structures are analyzed in terms of the number of clusters, the radii of micelle, core and shell, and the density profiles of residues. A three-step process is proposed for the assembly: small clusters are initially aggregated and then merged into large clusters, eventually micelles are formed. The effects of simulation box size and peptide concentration are examined in detail. It is found that the micellar structures and microscopic properties are essentially independent of box size. With increasing concentration, quasi-spherical micelles change to elongated shape and micelle size generally increases. The simulation study provides microscopic insight into the assembly process of FA32 peptide and the microscopic structures.

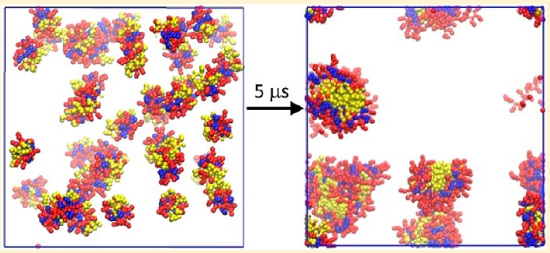

1. INTRODUCTION

High-efficacy drug delivery is of central importance for therapeutic treatment.[1] A number of materials including polymers and liposomes have been examined as carriers for drug delivery because of their self-assembly nature.[2] For example, amphiphilic polymers with hydrophilic and hydrophobic blocks can form a wide variety of morphologies, such as micelles, vesicles, tubes, and fibers.[3] This is attributed to the assembly of hydrophobic blocks, which minimizes the unfavorable interactions with water. The morphologies formed can be effectively utilized as carriers for controlled and targeted drug delivery.[4]

Composed of naturally occurring hydrophilic and hydrophobic amino acids, amphiphilic peptides are receiving considerable interest for drug delivery.[5] They are biodegradable and biocompatible, which are important characteristics for ideal drug carriers.[6] The assembled structures by peptides are pH-sensitive; additionally, the size, stability, and permeability can be fine-tuned by tailoring peptide sequence, length, and other solution conditions.[7] Experimental studies have been conducted to examine the self-assembly of various peptides. Zhang et al. observed that short peptides such as A_6D, V_6D, V_6D_2, and L_6D_2 formed nanotubes and fibers, and the nanotubes were 30−50 nm in diameter and several micrometers in length.[8] By varying the composition of V_6D_2 to V_5DVD and $V_4D_2V_2$, Adams et al. found the morphologies changed from nanotubes to fibers and tapes.[9] This study suggests the critical need in the careful design of peptide sequence and the purification of peptide sample, which plays a key role in the observed morphology. Xu et al. examined the effect of hydrophobic residues on the assembly of three peptides (A_3K, A_6K, and A_9K), and the morphology was found to change from sheets to fibers upon increasing hydrophobic segments.[10] In a recent study, Wiradharma et al. observed the formation of micelles by a peptide namely FA32 $[(AF)_6H_5K_{15}]$, which exhibited simultaneous delivery of drugs and genes.[11,12]

With ever-growing computational resources, molecular simulation has played an increasingly important role in physical and chemical sciences.[13] Simulation at a molecular level can provide microscopic understanding that otherwise is experimentally intractable or difficult to obtain, and thus elucidate underlying physics from bottom-up. Toward this end, a few simulation studies have been reported on the self-assembly of peptides, although not so extensively as compared to experimental studies. Hall and co-workers simulated the fibril formation of random-coiled polyalanine and the aggregation of polyglutamine peptides.[14,15] Frederix et al. examined the aggregation of dipeptides aiming to develop predictive simulation tools for dipeptide assembly.[16] Guo et al. simulated the assembly of diphenylalanine and found vesicles changed to nanotubes/bilayers upon changing peptide concentration.[17] Yethiraj and co-workers examined the driving force for association of peptides and amphiphilic molecules, and demonstrated that the driving force is sensitive to con-

Received: June 17, 2013
Revised: July 24, 2013

   dx.doi.org/10.1021/jp4059752 | J. Phys. Chem. B XXXX, XXX, XXX−XXX

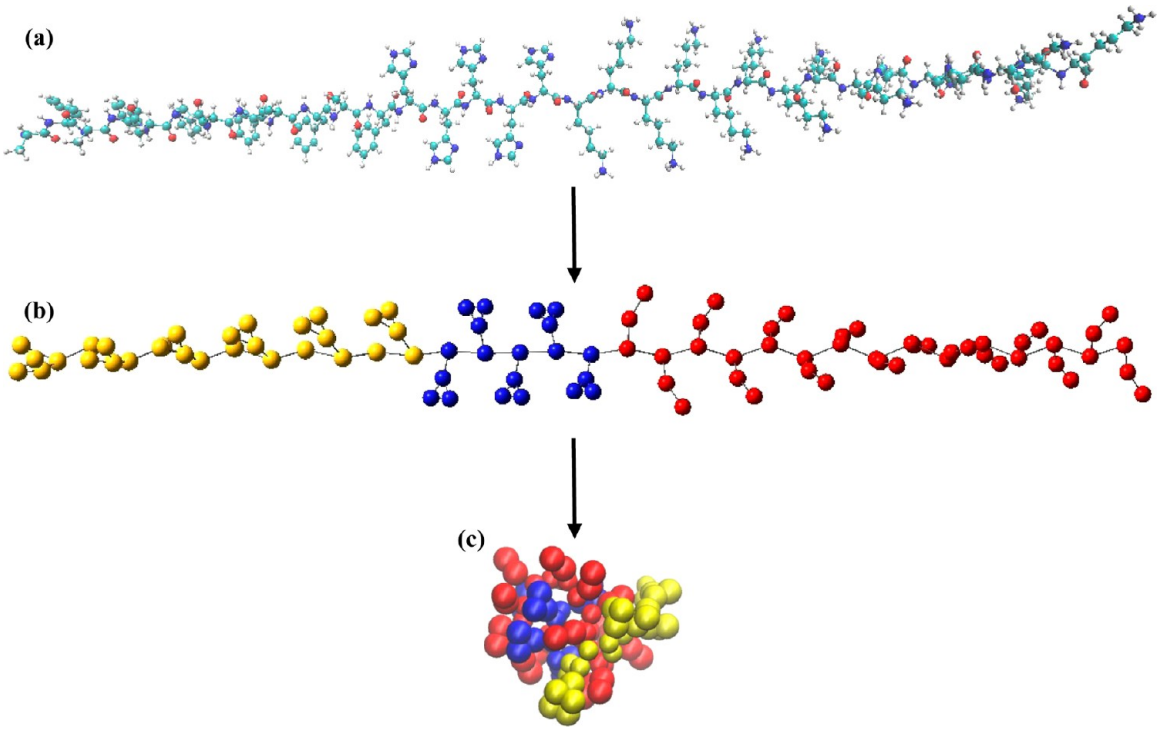

Figure 1. (a) Atomistic representation of FA32 peptide. N: blue, O: red, C: cyan, and H: white. (b) CG representation of FA32 peptide using the MARTINI model. Ala and Phe: yellow, His: blue, and Lys: red. (c) Aggregated structure of FA32 peptide.

ditions.[18,19] Combining simulation and experimental techniques, Hauser et al. examined the assembly of tri- to hexapeptides into coiled fibers.[20] Schatz and co-workers simulated the formation of fibers from peptide amphiphile (SLSLAAAEIKVAV), which initially assembled into micelles and then switched to fibers.[21,22]

It still remains a challenge on quantitative understanding of the self-assembly and morphology transition of peptides. Nevertheless, such understanding is indispensable for tuning the morphologies formed by peptides and designing specific peptides for efficient drug delivery. In this study, the self-assembly of peptide FA32 is simulated at a microscopic scale. As mentioned above, FA32 can assemble into micelle and appears as a promising delivery carrier.[11,12] Specifically, the assembly of FA32 was experimentally tested at concentrations above 40 mg/L, and the micelle formed had a radius of approximately 50 nm.

For practical application and further development, the assembly mechanism of FA32 needs to be better understood from bottom-up. In Section 2, the simulation model and method implemented are descried. In Section 3, two sets of simulation results are presented. One set is based on different box sizes (11, 15, and 18 nm) but with a close peptide concentration, attempting to evaluate the effect of box size. The other set is to examine the effect of peptide concentration with different peptides in 18 nm box. A number of characteristic parameters, such as the number of clusters, the radii of micelle, core and shell, and the density profiles of residues are used to analyze the assembly process and micellar structure of FA32. Finally, the concluding remarks are summarized in Section 4.

2. MODEL AND METHODS

Figure 1(a) illustrates a single chain of FA32, which consists of 32 amino acids $[(AF)_6H_5K_{15}]$. A and F are hydrophobic alanine (Ala) and phenylalanine (Phe), H is amphiphilic histidine (His), and K is hydrophilic lysine (Lys). It is computationally very expensive to conduct atomistic simulation for the self-assembly of such a long peptide, because self-assembly usually occurs in a microsecond time scale or even longer.[23,24] As an alternative, coarse-grained (CG) simulation is adopted in this study. In the CG modeling, the number of degrees of freedom is reduced by mapping several atoms as a bead. Although the atomistic details are lost, the essential molecular features are maintained in the CG mapping. Consequently, the simulation time scale can be accelerated. Here, FA32 is represented by the MARTINI modeling, which is a widely used CG protocol for lipids,[25] biomolecules,[26,27] and carbohydrates.[28] On average, the MARTINI modeling implements 4:1 mapping for linear molecules and 2/3:1 mapping for cyclic compounds. The interaction types are divided into polar (P), nonpolar (N), apolar (C), and charged (Q). These four types are further classified into 18 types of interaction sites based on hydrogen bonding capability and polarity, allowing the close representation for chemical structures of amino acids.

By using the MARTINI model, FA32 is mimicked by 95 beads in single chain, as shown in Figure 1(b). Nevertheless, the chain shown is in a physically unrealistic extended conformation. To examine its conformation in a solution, molecular dynamics (MD) simulation was carried out for a single FA32 chain in 11 nm box. Specifically, the FA32 chain was solvated in water and electrically neutralized by adding Cl^- ions. Both water and Cl^- were also represented by the MARTINI model. The MD simulation was performed with GROMACS package (version 4.5.3).[29] Within 100 ns, the extended FA32 chain was folded into an aggregated structure as shown in Figure 1(c). This aggregated structure was subsequently used to build two sets of simulation systems for assembly. As listed in Tables 1 and 2, the first set used three

dx.doi.org/10.1021/jp4059752 | J. Phys. Chem. B XXXX, XXX, XXX−XXX

Table 1. Three Different Box Sizes

no.	L_b (nm)	N_p	C_p (mg/mL)
1	11	10	76.7
2	15	26	73.1
3	18	44	78.0

Table 2. Nine Different Peptide Concentrations in an 18 nm Box

no.	N_p	C_p (mg/mL)
1	12	20.7
2	18	31.2
3	24	41.9
4	30	52.5
5	36	63.4
6	42	74.3
7	48	85.5
8	54	96.5
9	60	107.5

different box sizes (L_b = 11, 15, and 18 nm) with a close peptide concentration, whereas the second set had nine different peptide chains (N_p = 12, 18, 24, 30, 36, 42, 48, 54, and 60) in 18 nm box. From these two sets of systems, the effects of box size and peptide concentration were separately examined.

For each system, energy minimization was initially conducted using the steepest descent method with a maximum step size of 0.005 nm and a force tolerance of 10 kJ mol^{-1} nm^{-1}. Then NPT simulation was performed. The velocities were assigned according to the Maxwell–Boltzmann distribution at 310 K. Temperature was kept at 310 K by the Berendsen method[30] with a time constant of 1 ps, and pressure was maintained at 1 bar with a time constant of 6 ps and a compressibility of 3×10^{-4} bar^{-1}. In all three dimensions, the periodic boundary conditions were applied. The nonbonded Lennard–Jones (LJ) and electrostatic interactions were calculated using a cutoff of 1.2 nm. Furthermore, the standard shift function in GROMACS was used to reduce undesired noise.[29] Specifically, the LJ potential and electrostatic potentials were shifted to zero

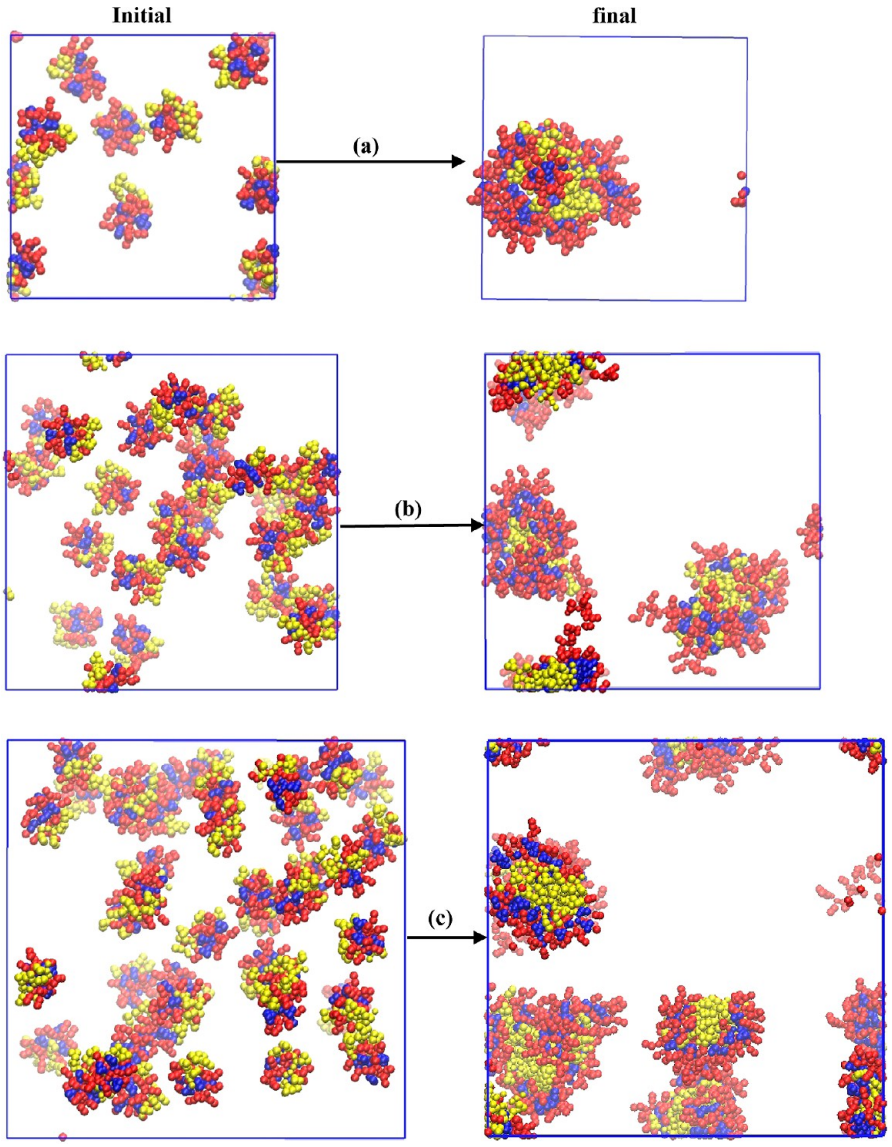

Figure 2. Initial and final snapshots (a) 10 peptides in an 11 nm box (b) 26 peptides in a 15 nm box (c) 44 peptides in an 18 nm box. Ala and Phe: yellow, His: blue, Lys: red. Water and Cl^- ion are not shown for clarity.

dx.doi.org/10.1021/jp4059752 | J. Phys. Chem. B XXXX, XXX, XXX–XXX

Table 3. Number of Micelles, Peptides Per Micelle, $R_{micelle}$, R_{core}, and R_{shell} in Three Box Sizes

L_b (nm)	number of micelles	peptides per micelle	$R_{micelle}$ (nm)	R_{core} (nm)	R_{shell} (nm)
11	1	10	3.43 ± 0.12	2.31 ± 0.07	1.11 ± 0.15
15	3	9 ± 1	3.27 ± 0.08	2.13 ± 0.07	1.14 ± 0.07
18	5	9 ± 4	3.22 ± 0.05	2.15 ± 0.03	1.07 ± 0.07

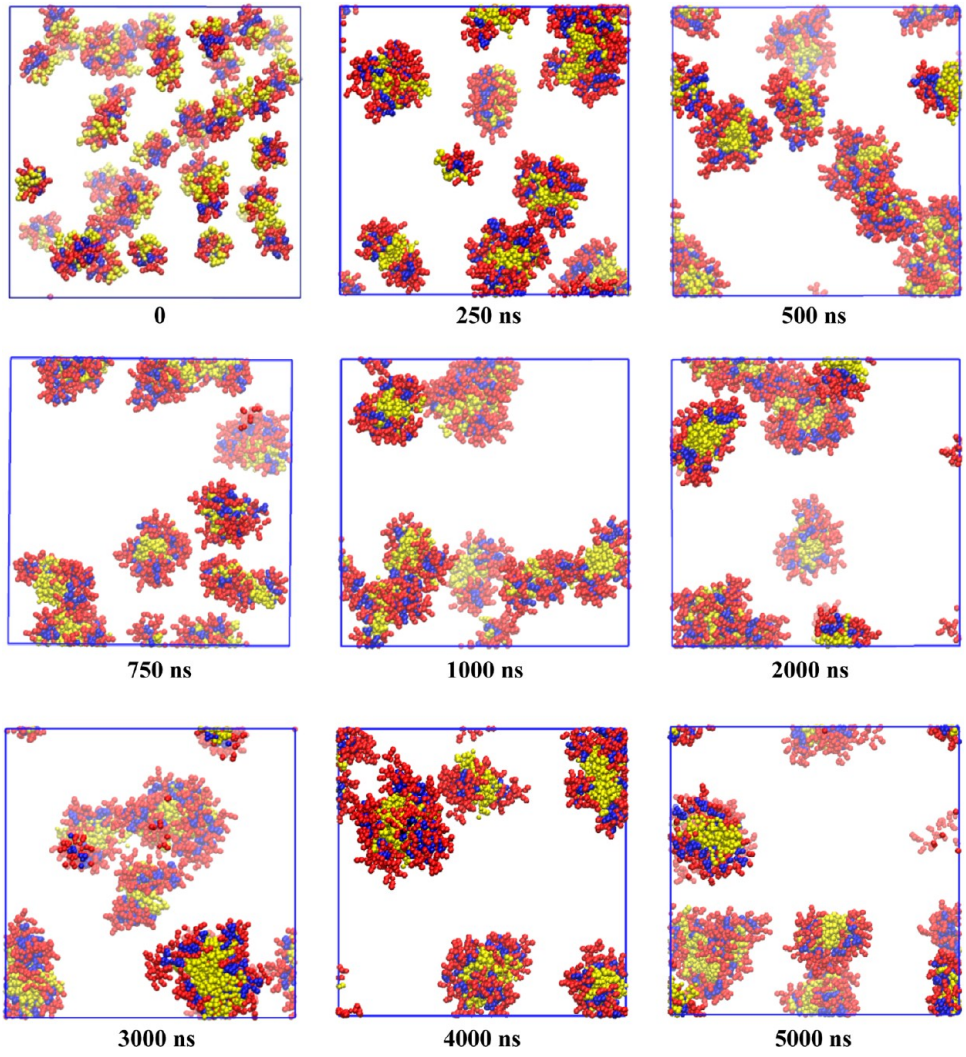

Figure 3. Snapshots for 44 peptides in an 18 nm box at different time intervals.

from 0.9 and 0.0 nm, respectively, to the cutoff distance (1.2 nm). A time step of 20 fs was used and trajectory was saved every 200 ps for analysis. The simulation duration was 5 μs, which is equivalent to an effective time of 20 μs. In the discussion below, we use the actual simulation time rather than the effective one unless specifically stated. The average values presented were calculated based on the last 1 μs.

3. RESULTS AND DISCUSSION

All simulation results presented are at 310 K (~37 °C), which is the temperature in the human body, as experimentally tested.[11,12] We first examine the effect of box size and then the effect of peptide concentration. For both cases, the assembly process and equilibrium structure are characterized by the number of clusters, the radii of micelle, core, and shell, as well as the density profiles of residues.

3.1. Effect of Box Size. The effect of box size is examined by simulation in three boxes with size L_b = 11, 15, and 18 nm. The peptide concentration in the three cases is close to 75 mg/mL. It should be noted that the concentration used in simulation is usually much higher than experimentally conducted.[11,12] The reason is that assembly is a long time scale process, and high concentration is often needed to promote the occurrence of assembly and reduce thermal noise.[17] This is similar to our recent simulation studies for liquid chromatographic separation of amino acids in a protein crystal and a metal−organic framework, respectively, where the external force assigned was higher than practically adopted.[31,32]

Figure 2 shows the initial and final snapshots of the three systems with different L_b. Water and Cl^- ion are not shown for clarity. Obviously, quasi-spherical micelles are formed in all the three systems. Hydrophobic Ala and Phe (yellow) constitute the core, hydrophilic Lys (red) forms the shell, and amphiphilic His (blue) is located at the interface. At the end of simulation, there are 1, 3, and 5 micelles formed in 11, 15, and 18 nm boxes, respectively. Thus, the number of micelles is

dx.doi.org/10.1021/jp4059752 | J. Phys. Chem. B XXXX, XXX, XXX−XXX

approximately proportional to box volume. Table 3 lists the number of peptides per micelle. In 11 nm box, the micelle contains 10 peptides; in 15 and 18 nm boxes, about 9 peptides exist in each micelle.

To better understand the assembly process, Figure 3 shows the snapshots for 44 peptides in 18 nm box at different time intervals. A video for the assembly of 44 peptides in 18 nm box is illustrated in the Supporting Information, SI. Initially (0 ns), each peptide exists individually in the system. At an early stage of simulation (250 ns), neighboring peptides aggregate into small clusters with hydrophobic residues residing in the interior. This implies that when hydrophobic residues move close, peptide chains start to aggregate and form clusters because of hydrophobic interactions.[11] Along with simulation (500−1000 ns), small clusters merge into large clusters. From 2000 ns till the end of simulation (5000 ns), 5 micelles are present and this number remains nearly the same. Therefore, the assembly can be considered as a *three-step process*: aggregation of small clusters, then large clusters, and eventually formation of micelles. In the last step, micelles reach equilibrium structure and cannot further aggregate even when the hydrophilic shells of two micelles come into contact. This might be due to the repulsion between positively charged Lys resides, which is unfavorable for micellization. Although Figure 3 is for 44 peptides in an 18 nm box, a similar process is also observed in the other two boxes (10 peptides in 11 nm box and 26 peptides in 15 nm box).

To quantitatively characterize the observed assembly process, two peptide chains are classified into the same cluster if the distance between any hydrophobic beads of the two chains is less than 0.7 nm. Figure 4 shows the number of clusters (N_c) as

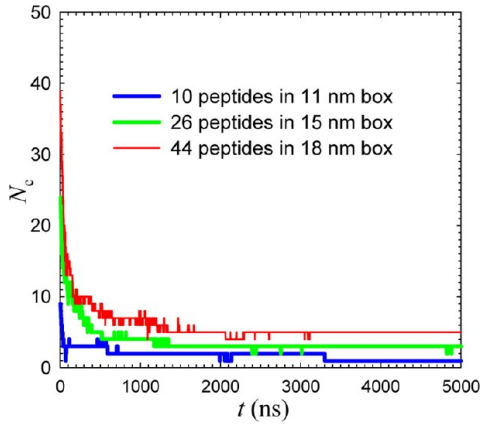

Figure 4. Number of clusters versus time for 10, 26, and 44 peptides in 11, 15, and 18 nm boxes, respectively.

a function of simulation time t in three boxes. At t = 0, N_c is large because each peptide exists individually. N_c decreases rapidly within 100 ns in 11 nm box, and within 400−500 ns in 15 and 18 nm boxes. This is attributed to the formation of small clusters by peptide chains in the first step. In the second step, small clusters merge into large ones, and N_c decreases gradually. In the third step, micelles are formed and afterward N_c is nearly constant. Specifically, N_c are equal to 1, 3, and 5 in the three boxes, consistent with the number of micelles visualized in Figure 2. With a closer look, we see small fluctuations of N_c in the third step. In 18 nm box, e.g., N_c fluctuates from 5 to 4 during 3000−3200 ns. This corresponds to the occurrence of close contact of two micelles during assembly. Despite the fluctuations, the constant value of N_c remains well and thus the micelles are stable.

The micelle formed by FA32 peptide consists of hydrophobic core and hydrophilic shell. The radii of micelle and core are estimated by the following:[33]

$$R_{\text{micelle}} = \sqrt{\frac{1}{N}\sum_{i=1}^{N}(r_i - r_{\text{com}})^2} \quad (1)$$

$$R_{\text{core}} = \sqrt{\frac{1}{N}\sum_{i=1}^{N}(r_{\text{HPB},i} - r_{\text{com}})^2} \quad (2)$$

where N is the number of peptides in the micelle, r_{com} is the center-of-mass (COM) of the micelle, r_i and $r_{\text{HPB},i}$ are the positions of outermost bead and hydrophobic bead in each peptide chain. The radius or thickness of shell (R_{shell}) is the difference between R_{micelle} and R_{core},

$$R_{\text{shell}} = R_{\text{micelle}} - R_{\text{core}} \quad (3)$$

Figure S1 of the SI illustrates the R_{micelle}, R_{core}, and R_{shell} versus time in three boxes with L_b = 11, 15, and 18 nm. The profiles generally remain flat with time, suggesting equilibrium is reached. From the last 1000 ns trajectory, the time-averaged values of the R_{micelle}, R_{core}, and R_{shell} are listed in Table 3. The R_{micelle}, R_{core}, and R_{shell} are close in the three boxes and in the ranges of 3.2−3.4 nm, 2.1−2.3 nm, and 1.0−1.1 nm, respectively. This reveals that they are essentially independent of box size, and the small difference among the three boxes can be attributed to the slight different number of peptide chains present in each micelle.

The R_{micelle} in Figure S1 of the SI is averaged of all micelles present in a system. However, different micelles may possess unequal size or even a micelle may change size due to fluctuation, thus it is instructive to examine the distribution of R_{micelle}. Figure 5 shows the distributions of R_{micelle} in three boxes with L_b = 11, 15, and 18 nm. We should point out that in 11 nm box, only one micelle was observed in the final snapshot (see Figure 2a). However, the side chains of Lys exhibit large fluctuations and hence R_{micelle} distributes between 3.1 and 3.7 nm. In 15 nm box, R_{micelle} ranges from 2.8 to 3.7 nm. In 18 nm box, R_{micelle} is distributed more widely, from 2.4 to 4.0 nm. Thus, the distribution becomes wider with increasing box size due to the formation of more micelles and larger fluctuations in micelle size. Compared to a experimentally measured value (about 50 nm),[11,12] the predicted R_{micelle} is much smaller. The possible reasons are (1) the simulation is not sufficiently long and prohibits the formation of very larger micelles (2) the force field adopted might not be accurate to describe FA32 peptide. Similar magnitude of deviation in the size of spherical vesicles formed by diphenylalanine was also observed between simulation and experimental studies.[17]

FA32 consists of four types of residues including Ala, Phe, His, and Lys. To examine their locations in a micelle, the density profiles were evaluated as a function of distance from the COM. For the case of 26 peptides in 15 nm box, 3 micelles are formed and the density profiles are shown in Figure 6. Apparently, the density profiles of 3 micelles are similar, with clear core and shell indicating the 3 micelles possess nearly identical structure. Specifically, hydrophobic Ala and Phe reside in the core, mostly in the range of 0−1.5 nm. In particular, Phe has the highest density at the COM. Again, this confirms the observation in Figure 2 that the formation of micelle core is due

dx.doi.org/10.1021/jp4059752 | J. Phys. Chem. B XXXX, XXX, XXX−XXX

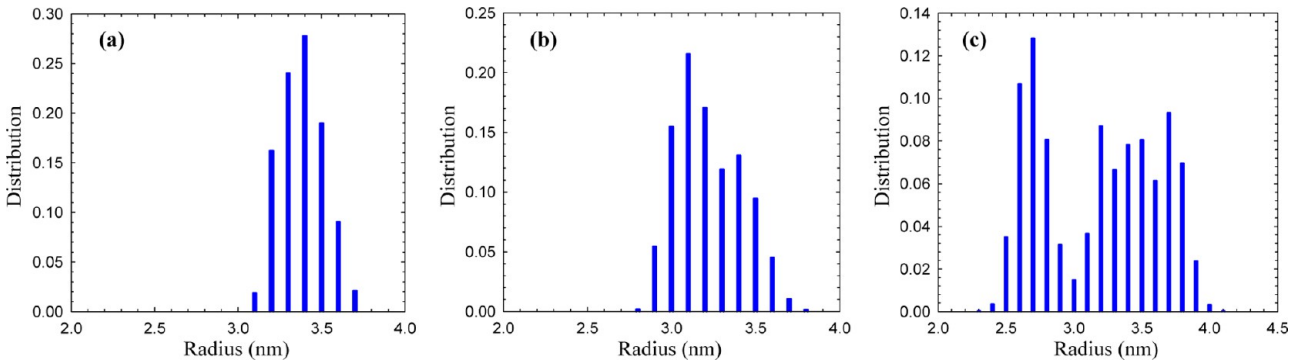

Figure 5. Distributions of $R_{micelle}$ for (a) 10 peptides in an 11 nm box (b) 26 peptides in a 15 nm box (c) 44 peptides in an 18 nm box.

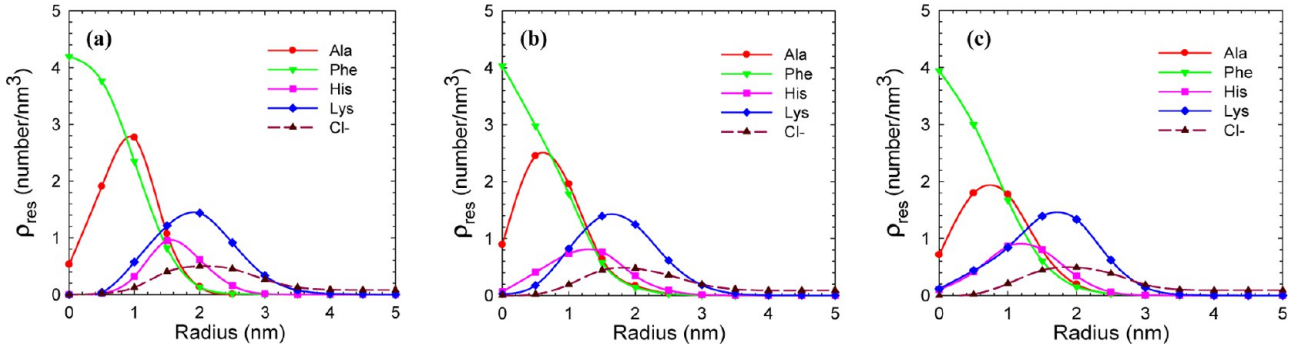

Figure 6. Density profiles of micelles for 26 peptides in a 15 nm box. The micelles contain 10, 8, and 8 peptides in (a), (b), and (c), respectively.

to hydrophobic interactions. Hydrophilic Lys is located in the shell, preferentially at 1−3 nm. For amphiphilic His, a pronounced density is observed at 1.5 nm, which is the interface. Furthermore, most Cl^- ions are located at 1−3 nm for the neutralization of Lys. The density profiles in 11 and 18 nm boxes exhibit features similar to Figure 6.

From the above simulation results in three boxes with different sizes but a close peptide concentration, we can conclude that the number of micelles is proportional to box volume, the number of peptides per micelle is approximately the same in the three boxes, the $R_{micelle}$, R_{core}, and R_{shell} are nearly identical despite different distributions, and the density profiles are also similar. Therefore, the assembled structures and microscopic properties are essentially independent of box size.

3.2. Effect of Peptide Concentration. Peptide concentration is one important factor to govern assembly. The effect of peptide concentration is examined by simulating nine systems with different number of peptides N_p in 18 nm box, as listed in Table 2. From the final snapshots illustrated in Figure 7, the numbers of micelles formed are estimated to be 2, 3, 3, 4, 4, 6, 3, 5, and 5 for N_p = 12, 18, 24, 30, 36, 42, 48, 54, and 60 in the nine systems, respectively. Apparently, the number of micelles appears to be a complex function of N_p. With increasing N_p from 12 to 42, the number of micelles increases from 2 to 6, and the micelles exhibit quasi-spherical shape. However, the number decreases to 3 for N_p = 48, and then increases again to 5 with further increasing N_p to 54 and 60. The decrease is due to the formation of elongated micelles as more peptides are involved in micellization. It is interesting to note that a micelle with more than 15 peptides exhibits irregular nonspherical shape. For example, several micelles consist of 20 peptides and are elongated in one direction. To quantitatively analyze the effect of peptide concentration, three systems with N_p = 18, 36, and 60 are chosen and further discussed below.

Figure 8 shows the number of clusters (N_c) for N_p = 18, 36, and 60. The three-step assembly mechanism discussed above is also observed here. For each N_p, small clusters are initially aggregated and then merged into large clusters, and finally formed micelles. With increasing N_p, the value of N_c increases. Specifically, 3 micelles are formed at 1000 ns for N_p = 18; while for N_p = 36 and 60, 4, and 5 micelles are formed at about 1500 ns. However, small fluctuations are observed afterward because the micelles may move close or away. Consequently, the number of micelles, as well as fluctuations, increases with increasing N_p.

Figure S2 in the Supporting Information plots the radii of micelle ($R_{micelle}$), core (R_{core}), and shell (R_{shell}) for N_p = 18, 36, and 60. Equilibrium stage is reached for each N_p, and the time-averaged values are listed in Table 4. With increasing N_p from 18, 36 to 60, the $R_{micelle}$, R_{core}, and R_{shell} increase from 2.92 to 3.61 nm, 1.97 to 2.37 nm, and 0.94 to 1.23 nm, respectively. This is because the micelle contains more peptides for a greater N_p. As listed in Table 4, the number of peptides per micelle increases from 6, 9 to 12 upon increasing N_p from 18, 36 to 60.

The distributions of $R_{micelle}$ for N_p = 18, 36, and 60 are shown in Figure 9. For N_p = 18, the $R_{micelle}$ is distributed between 2.3 and 3.4 nm. The distribution is in the range of 2.6 and 3.7 nm for N_p = 36, 3.3 and 4.0 nm for N_p = 60. Apparently, the micelle size becomes lager with increasing N_p as the micelle contains more peptides.

Figure 10 shows the density profiles of micelles for N_p = 18, 36, and 60. The three micelles considered contain 7, 10, and 12 peptides, respectively. All of the density profiles reveal the formation of hydrophobic core and hydrophilic shell. For the micelle with 7 peptides, Ala and Phe reside over the range of 0−1.5 nm, and similar to Figure 6, Phe exhibits the highest

dx.doi.org/10.1021/jp4059752 | J. Phys. Chem. B XXXX, XXX, XXX−XXX

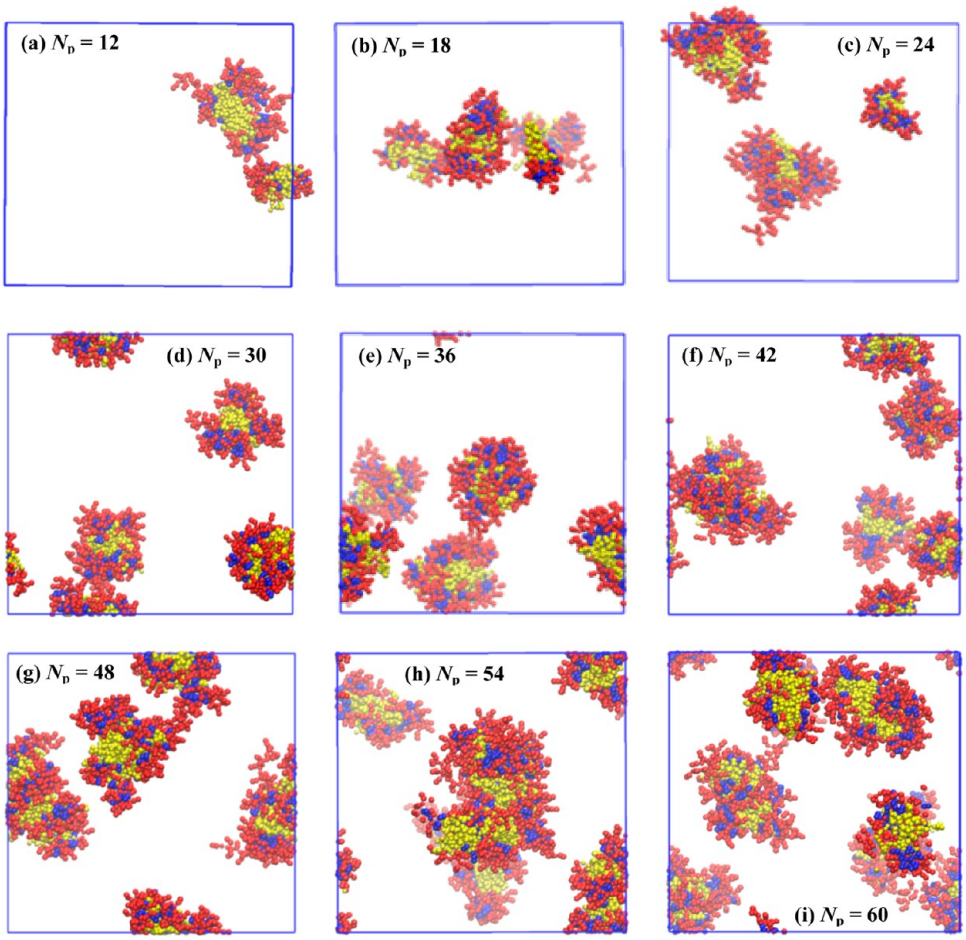

Figure 7. Final snapshots for different peptide concentrations in an 18 nm box. From (a) to (i), N_p = 12, 18, 24, 30, 36, 42, 48, 54, 60, respectively.

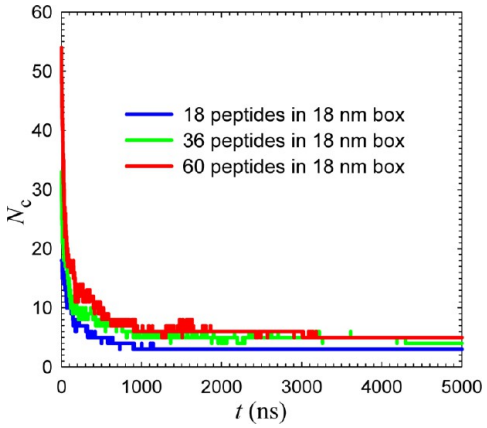

Figure 8. Number of clusters versus time for 18, 36, and 60 peptides in an 18 nm box.

density at the COM. Lys is located mostly in the shell beyond 1.5 nm and His is preferentially at the interface of about 1.5 nm. As a comparison, the profiles for the micelles with 10 and 12 peptides are shifted toward right (further away from the COM). This is consistent with the observation in Figure 9, i.e, the micelle size becomes larger with more peptides present.

The simulation results with different peptide concentrations reveal that the number of micelles formed is a complex function of peptide concentration. With increasing peptide concentration, the micellar shape changes from quasi-spherical to elongated, the number of peptides per micelle increases, the $R_{micelle}$, R_{core}, and R_{shell} also increase, and the density profiles are extended away from the center of micelle.

Table 4. Number of Micelles, Peptides Per Micelle, $R_{micelle}$, R_{core}, and R_{shell} in an 18 nm Box

N_p	number of micelles	peptides per micelle	$R_{micelle}$ (nm)	R_{core} (nm)	R_{shell} (nm)
12	2	6	3.12 ± 0.11	2.07 ± 0.08	1.05 ± 0.13
18	3	6	2.92 ± 0.06	1.97 ± 0.05	0.94 ± 0.08
24	3	8	3.13 ± 0.07	2.06 ± 0.07	1.07 ± 0.08
30	4	7 ± 1	3.18 ± 0.06	2.02 ± 0.03	1.15 ± 0.07
36	4	9	3.29 ± 0.05	2.17 ± 0.05	1.19 ± 0.05
42	6	7	3.04 ± 0.09	2.02 ± 0.06	1.03 ± 0.08
48	3	16	3.48 ± 0.53	2.26 ± 0.35	1.22 ± 0.18
54	5	11 ± 1	3.55 ± 0.05	2.37 ± 0.04	1.17 ± 0.05
60	5	12	3.61 ± 0.04	2.37 ± 0.03	1.23 ± 0.04

4. CONCLUSIONS

The self-assembly of amphiphilic peptide FA32 has been investigated using coarse-grained simulation. Micelles are observed to form, in which Ala and Phe are located in the core, Lys in the shell, and His at the interface. A three-step process is proposed for the assembly. Initially, peptides aggregate into small clusters, then merge into large clusters, and eventually form micelles. Once equilibrium is reached, the micelle structure remains relatively stable. The interactions

dx.doi.org/10.1021/jp4059752 | J. Phys. Chem. B XXXX, XXX, XXX−XXX

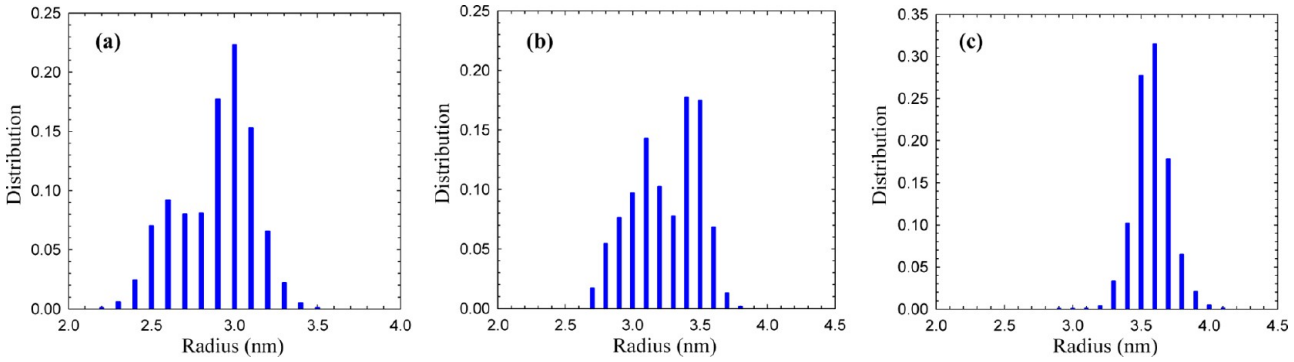

Figure 9. Distributions of $R_{micelle}$ for (a) 18, (b) 36, and (c) 60 peptides in an 18 nm box.

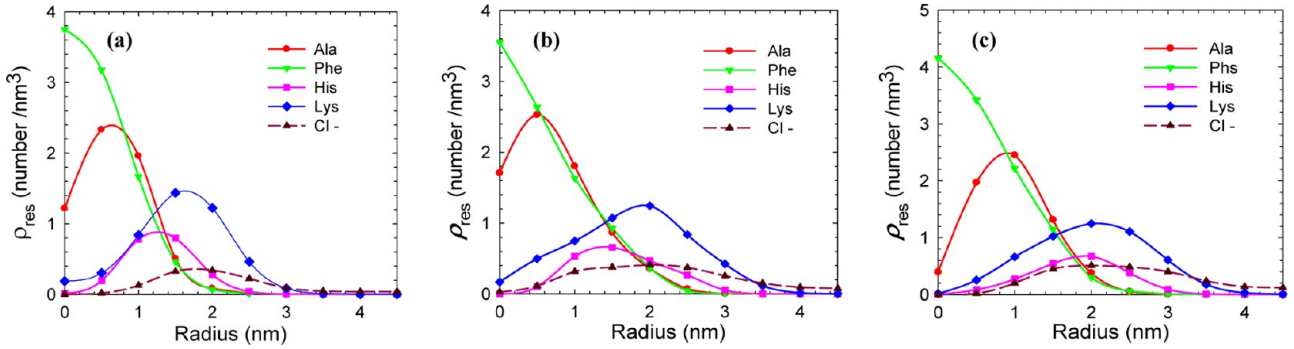

Figure 10. Density profiles of micelles for 18, 36, and 60 peptides in an 18 nm box. The micelles contain 7, 10, and 12 peptides in (a), (b), and (c), respectively.

between hydrophobic residues are crucial for the aggregation of small cluster and subsequent micellization. In three simulation boxes with sizes of 11, 15, and 18 nm, quasi-spherical micelles are formed. At a given peptide concentration, the number of peptides per micelle remains nearly constant. The radii of micelle, core, and shell are approximately the same in the three boxes, within 3.2−3.4 nm, 2.1−2.3 nm, and 1.0−1.1 nm, respectively. The density profiles of residues in the micelles are also similar. These results reveal that the assembled structures are largely independent of box size. In nine systems with different peptide concentrations, quasi-spherical micelles are observed to change to elongated shape at high concentrations. With increasing concentration, the micelle size increases, as well as the radii of micelle, core, and shell.

It should be noted that the assembly depends on several factors such as system size, concentration, temperature, pH value, ionic strength, and so forth. While this study is focused on the effects of system size and concentration, other factors will be examined in our future study toward more comprehensive understanding of the assembly process.

■ ASSOCIATED CONTENT

Supporting Information

A video for the assembly of 44 peptides in 18 nm box; the radii of micelle, core, and shell. This material is available free of charge via the Internet at http://pubs.acs.org.

■ AUTHOR INFORMATION

Corresponding Author

*E-mail: chejj@nus.edu.sg.

Notes

The authors declare no competing financial interest.

■ ACKNOWLEDGMENTS

The authors gratefully acknowledge the National University of Singapore and the Ministry of Education of Singapore for financial support, and Prof. Yen Wah Tong for helpful discussion.

■ REFERENCES

(1) Santini, J. T., Introduction to Drug Delivery Technology. *Chem. Eng. Prog.* March **2013**, pp 19-23.

(2) Langer, R.; Tirrell, D. A. Designing Materials for Biology and Medicine. *Nature* **2004**, *428*, 487−492.

(3) Blanazs, A.; Armes, S. P.; Ryan, A. J. Self-Assembled Block Copolymer Aggregates: From Micelles to Vesicles and Their Biological Applications. *Macromol. Rapid Commun.* **2009**, *30*, 267−277.

(4) Zhang, X. X.; Eden, H. S.; Chen, X. Y. Peptides in Cancer Nanomedicine: Drug Carriers, Targeting Ligands and Protease Substrates. *J. Controlled Release* **2012**, *159*, 2−13.

(5) Gonzalez-Aramundiz, J. V.; Lozano, M. V.; Sousa-Herves, A.; Fernandez-Megia, E.; Csaba, N. Polypeptides and Polyaminoacids in Drug Delivery. *Exp. Opin. Drug Deliv.* **2012**, *9*, 183−201.

(6) Langer, R. Biocompatibility and Drug Delivery Systems. *Chem. Sci.* **2010**, *1*, 441−446.

(7) Zhao, X. B.; Pan, F.; Xu, H.; Yaseen, M.; Shan, H. H.; Hauser, C. A. E.; Zhang, S. G.; Lu, J. R. Molecular Self-Assembly and Applications of Designer Peptide Amphiphiles. *Chem. Soc. Rev.* **2010**, *39*, 3480−3498.

(8) Vauthey, S.; Santoso, S.; Gong, H. Y.; Watson, N.; Zhang, S. G. Molecular Self-Assembly of Surfactant-Like Peptides to Form Nanotubes and Nanovesicles. *Proc. Natl. Acad. Sci. U.S.A.* **2002**, *99*, 5355−5360.

(9) Adams, D. J.; Holtzmann, K.; Schneider, C.; Butler, M. F. Self-Assembly of Surfactant-Like Peptides. *Langmuir* **2007**, *23*, 12729−12736.

(10) Xu, H.; Wang, J.; Han, S. Y.; Wang, J. Q.; Yu, D. Y.; Zhang, H. Y.; Xia, D. H.; Zhao, X. B.; Waigh, T. A.; Lu, J. R. Hydrophobic-

Region-Induced Transitions in Self-Assembled Peptide Nanostructures. *Langmuir* **2009**, *25*, 4415−4123.
(11) Wiradharma, N.; Tong, Y. W.; Yang, Y. Y. Design and Evaluation of Peptide Amphiphiles with Different Hydrophobic Blocks for Simultaneous Delivery of Drugs and Genes. *Macromol. Rapid Commun.* **2010**, *31*, 1212−1217.
(12) Wiradharma, N.; Tong, Y. W.; Yang, Y. Y. Self-Assembled Oligopeptide Nanostructures for Co-Delivery of Drug and Gene with Synergistic Therapeutic Effect. *Biomaterials* **2009**, *30*, 3100−3109.
(13) Chakraborty, A. *Molecular Modeling and Theory in Chemical Engineering*. Academic Press: San Diego, 2001; Vol. *28*.
(14) Nguyen, H. D.; Hall, C. K. Molecular Dynamics Simulations of Spontaneous Fibril Formation by Random-Coil Peptides. *Proc. Natl. Acad. Sci. U.S.A.* **2004**, *101*, 16180−16185.
(15) Marchut, A. J.; Hall, C. K. Effects of Chain Length on the Aggregation of Model Polyglutamine Peptides. *Proteins* **2007**, *66*, 96−109.
(16) Frederix, P. W. J. M.; Ulijn, R. V.; Hunt, N. T.; Tuttle, T. Virtual Screening for Dipeptide Aggregation: Toward Predictive Tools for Peptide Self-Assembly. *J. Phys. Chem. Lett.* **2011**, *2*, 2380−2384.
(17) Guo, C.; Luo, Y.; Zhou, R. H.; Wei, G. H. Probing the Self-Assembly Mechanism of Diphenylalanine-Based Peptide Nanovesicles and Nanotubes. *ACS Nano* **2012**, *6*, 3907−3918.
(18) Wu, Z.; Cui, Q.; Yethiraj, A. Driving Force for the Association of Hydrophobic Peptides. *J. Phys. Chem. Lett.* **2011**, *2*, 1794−1798.
(19) Mondal, J.; Yethiraj, A. Driving Force for the Association of Amphiphilic Molecules. *J. Phys. Chem. Lett.* **2011**, *2*, 2391−2395.
(20) Hauser, C. A. E.; Deng, R.; Mishra, A.; Loo, Y.; Khoe, U.; Zhuang, F.; Cheong, D. W.; Accardo, A.; Sullivan, M. B.; Rieker, C.; Ying, J. Y.; Hauser, U. A. Natural Tri- to Hexapeptides Self-Assemble in Water to Amyloid B−Type Fiber Aggregates by Unexpected by Unexpected A-Helical Intermediate Structures. *Proc. Natl. Acad. Sci. U.S.A.* **2011**, *108*, 1361−1366.
(21) Lee, O. S.; Stupp, S. I.; Schatz, G. C. Atomistic Molecular Dynamics Simulations of Peptide Amphiphile Self-Assembly into Cylindrical Nanofibers. *J. Am. Chem. Soc.* **2011**, *133*, 3677−3683.
(22) Lee, O. S.; Cho, V.; Schatz, G. C. Modeling the Self-Assembly of Peptide Amphiphiles into Fibers Using Coarse-Grained Molecular Dynamics. *Nano Lett.* **2012**, *12*, 4907−4913.
(23) Klein, M. L.; Shinoda, W. Large-Scale Molecular Dynamics Simulations of Self-Assembling Systems. *Science* **2008**, *321*, 798−800.
(24) McCullagh, M.; Prytkova, T.; Tonzani, S.; Winter, N. D.; Schatz, G. C. Modeling Self-Assembly Process Driven by Nonbonded Interactions in Soft Materials. *J. Phys. Chem. B* **2008**, *112*, 10388−10398.
(25) Marrink, S. J.; de Vries, A. H.; Mark, A. E. Coarse Grained Model for Semiquantitative Lipid Simulations. *J. Phys. Chem. B* **2004**, *108*, 750−760.
(26) Marrink, S. J.; Risselada, H. J.; Yefimov, S.; Tieleman, D. P.; de Vries, A. H. The Martini Force Field: Coarse Grained Model for Biomolecular Simulations. *J. Phys. Chem. B* **2007**, *111*, 7812−7824.
(27) Monticelli, L.; Kandasamy, S. K.; Periole, X.; Larson, R. G.; Tieleman, D. P.; Marrink, S. J. The Martini Coarse-Grained Force Field: Extension to Proteins. *J. Chem. Theory Comput.* **2008**, *4*, 819−834.
(28) Lopez, C. A.; Rzepiela, A. J.; de Vries, A. H.; Dijkhuizen, L.; Hunenberger, P. H.; Marrink, S. J. Martini Coarse-Grained Force Field: Extension to Carbohydrates. *J. Chem. Theory Comput.* **2009**, *5*, 3195−3210.
(29) Hess, B.; Kutzner, C.; van der Spoel, D.; Lindahl, E. Gromacs 4: Algorithms for Highly Efficient, Load-Balanced, and Scalable Molecular Simulation. *J. Chem. Theory Comput.* **2008**, *4*, 435−447.
(30) Berendsen, H. J. C.; Postma, J. P. M.; Vangunsteren, W. F.; Dinola, A.; Haak, J. R. Molecular-Dynamics with Coupling to an External Bath. *J. Chem. Phys.* **1984**, *81*, 3684−3690.
(31) Hu, Z. Q.; Jiang, J. W. Separation of Amino Acids in Glucose Isomerase Crystal: Insight from Molecular Dynamics Simulations. *J. Chromat. A* **2009**, *1216*, 5122−5129.
(32) Hu, Z. Q.; Chen, Y. F.; Jiang, J. W. Liquid Chromatographic Separation in Metal−Organic Framework MIL-101: A Molecular Simulation Study. *Langmuir* **2013**, *29*, 1650−1656.
(33) Luo, Z. L.; Jiang, J. W. Ph-Sensitive Drug Loading/Releasing in Amphiphilic Copolymer PAE−PEG: Integrating Molecular Dynamics and Dissipative Particle Dynamics Simulations. *J. Controlled Release* **2012**, *162*, 185−193.